We SRS1 12

Imaging Hydrothermal Circulation Paths along the East Pacific Rise Using Elastic Wave-equation Based Inversion Technique

M. Marjanovic* (Institut de Physique du Globe de Paris (IPGP)), N. Fuji (IPGP), S.C. Singh (IPGP) & T. Belahi (IPGP)

SUMMARY

Along mid-ocean ridges, locations where hydrothermal fluids emerge onto the seafloor and potentially significant mineral ore bodies form, have been considered for future mineral exploitation. However, before the mining takes place at hydrothermal vents we need to better understand circulation paths of the fluids that are the main transporters of the minerals that eventually lead to important mineral accumulations. Here, for the first time, we apply elastic wave-equation tomography and full-waveform inversion to a 2-D seismic dataset collected along the East Pacific Rise, ridge system with abundant hydrothermal activity. Due to a large and robust Fresnel zone used in wave-equation tomography, we were able to start with a rough estimate of the initial velocity model. Consideration of complex seismic wave propagation phenomenon through elastic wave-equation modelling allowed us to image low velocity zones that can be tracked down to 1 km below the seafloor. We interpret them as up- or down-going paths of hydrothermal fluid circulation as they match with locations of high-temperature vents, previously mapped on the seafloor. Furthermore, higher velocity zones in the vicinity of two prominent vent fields may mark presence of mineral deposits.

Introduction

Hydrothermal circulation along divergent plate boundaries plays an important role in heat transfer between deep ocean and the Earth's lithosphere, resulting in formation of imposing hydrothermal vents. Mineral-enriched fluids that are emanated from these vents are supporting most incredible forms of life, which may tell us a story of the onset of life on our planet. In addition, they are loci of important massive sulphide ore deposits of base metals. Until now 330 sulphide deposits have been reported to reside at the bottom of the world's ocean. For some of them geochemists suggested significant presence of copper and zinc, but also gold and silver, which sparked interest of some of the mining companies to investigate possibility for future, economically feasible exploitation of hydrothermal vents.

Although the hydrothermal vents have economically interesting potential for mineral ore prospecting that will most certainly take place, we have no constraints on their internal structure, and their extent in depth, and thus no estimates on their exploitation potential. In addition, we have only a wage idea on hydrothermal fluids circulation patterns in the upper crust that lead to the formation of these accumulations.

Here, we use two wave-equation based inversion techniques: elastic wave-equation tomography (WET) and full-waveform inversion (FWI). The idea is to take advantage of large Fresnel zone of WET and detailed model resolving power of FWI to image characteristics of upper oceanic crust formed at the East Pacific Rise (EPR) ~9ºN, where a number of active and inactive vent fields are reported to exist. Our goal is to obtain seismic structure of several hundreds of metres of the upper crust and infer possible presence of hydrothermal fluids paths along the ridge axis, i.e. zero age crust. We use high-resolution 2-D multi-channel seismic line collected in 2008 as part of a 3-D seismic survey. In order to facilitate inversions, we carefully extrapolate the data acquired on the sea surface to ~100-200 m above the seafloor. Our results show presence of ~4 km wide (in along axis direction) low velocity zones that can be observed up to 1 km below the seafloor. Their distribution dove-tails with superficial distribution of vents and micro seismicity.

Data and methodology

Data acquisition **-** During *R/V Marcus G. Langseth* expedition MGL0812 conducted in 2008, swaths of reflection seismic data spanning the innermost portion of the EPR axis from Siqueiros to Clipperton Transform Fault were acquired. The signal was recorded using four solid-state 6 km long streamers, each with 468 channels, electrically coupled at 12.5 m. As a source of the seismic signal, two tuned air-gun arrays were used, each composed of nine guns, with volume 1650 in^3. Gun-array was deployed at 7.5 m, as well as the receivers along the streamer. The arrays were firing in

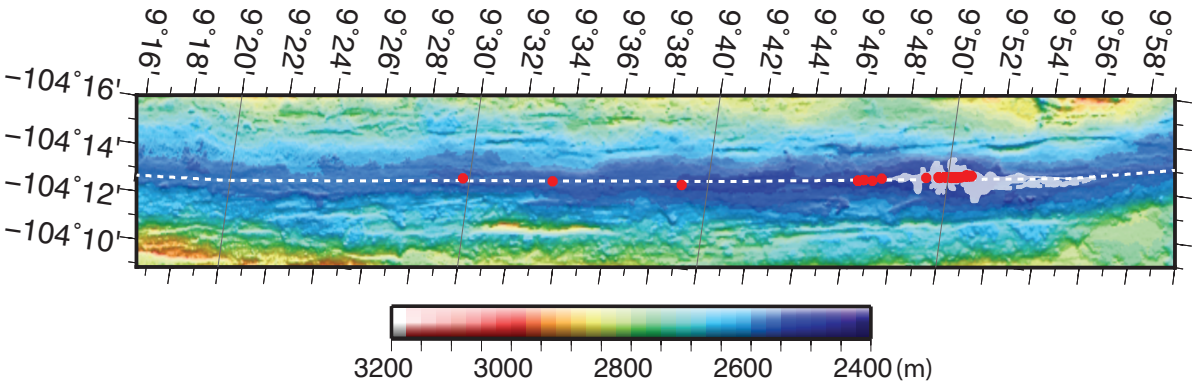

Figure 1 *Survey area. Track line axis2r1 from expedition MGL0812 used in this study. This line runs closest to the innermost axial zone (i.e. zero age crust). Background is a bathymetric image of the EM120 multibeam echo-sounder data collected during the same survey and gridded at 50 m. Outline of the 2005–2006 lava flow is from Fundis et al. (2010) is marked in shaded grey area. Red circles are locations of the hydrothermal vents.*

alternating mode, which for given four cables geometry resulted in a swath of seismic data composed of eight 2-D lines separated by 37.5 m, with shot spacing 75 m.
Here, upon examining all collected along-axis lines, for 2-D waveform modelling we chose to use data recorded along a portion of the axis2r1 extending between ~9º16' to 9º56'N, where topography effect is negligible (Figure 1). We combine two 2-D common-mid point lines recorded along cable 2 to obtain a line with 37.5 m shot interval.

Processing - To remove noise from the chosen 2-D seismic line, we first apply band-pass filter with cut-off frequencies 1-6-200-220 Hz. We then edit traces (to eliminate bad channels) and interpolate them. We interpolated missing shots by their two nearest shots. We then apply a 2-D filter(s) using LIFT techniques (Choo *et al.* 2004; Aghaei *et al. 2014*): i) we subdivide the data into low- (0-14-16 Hz), mid- (14-16-20-25 Hz) and high (20-25-200-220 Hz) frequency bands; ii) since the dominant noise for the EPR data is arising from frequencies of <15 Hz, we apply an FK filter to the low-frequency band. In addition, we apply surface consistent amplitude balancing since there are weak channels that do not originate from geology, and apply low-pass filter with corner frequencies of 25-30Hz. We then mute the data from ~1 s above the seafloor to 6.5 s. Since our inversion scheme treats 2-D data, we apply corrections for the 3-D effect (Pica *et al.,* 1990): correction for 3-D spherical geometric spreading to 2-D cylindrical geometric spreading; and correction for 3-D point source to a 2-D line source. The former correction is just a simple amplitude scaling by sqrt(t), whereas convolving the data by 1/sqrt(t) accommodates the latter one.

Wavefield extrapolation - In order to make inversions efficient and stable, we re-datum sources and receivers on the sea surface to about 100-200 m above the seafloor. Since Green's function in water can be approximated to be a simple delta function, we choose Kirchhoff integral approach (Berryhill, 1979). We validated its accuracy by conducting synthetic tests. We limit shot gather offsets to the range between 1875 m to 3750 m. Computational burdens limit us to use every 4th shot and thus for inversion we end up with 490 shots with 150 m spacing.
Prior to inversion we conduct far-field source signature modelling using Nucleus (Figure 2).

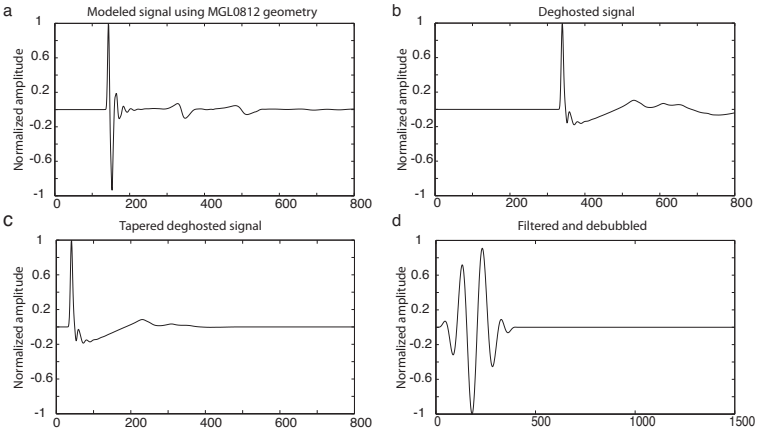

Figure 2 *Source wavelet. (a) Far-field source wavelet modelled in Nucleus. (b) Deghosted source wavelet. (c) Tapered source wavelet. (d) Filtered source wavelet.*

Inversions - Here, we use two elastic wave-equation inversion schemes, first WET (Luo & Schuster, 1991; Wang *et al.,* 2014) and then FWI (e.g. Shipp & Singh, 2002), both applied on wide-angle (mostly) refracted arrival(s). The above two techniques are based on a 2-D approximation of elastic wave equation that is solved using a time domain finite difference scheme, a fourth-order in space and second-order in time (Levander, 1988) with 12.5 m grid spacing and 1 ms time step.
WET minimises travel-time misfit measured by cross-correlation and it takes into account accurately the complex Fresnel zone of a certain phase. WET provides sufficient kinematic information for FWI to converge to a global minimum and avoid cycle skipping. Since the Fresnel zone is normally larger than that of FWI, we can start with poorly determined initial velocity models in WET. Here in this study, for example, we use 1-D velocity model obtained from extended seismic profiling (Vera *et al.,* 1990), along the entire length of the seismic line used in this study (Figure 3a). We designed appropriate time window, since we are particularly interested in wide-angle refracted phases. About 50 iterations were necessary to obtain ~16% of misfit reduction. The final velocity model obtained from WET (Figure 3b) is used as a starting model for FWI. During FWI, we use data filtered to a dominant frequency of 8 Hz (together with the source signal) and only use wide-angle arrivals. Finally, 20 iterations were run to obtain optimal results (Figure 3c). Shear wave velocity and density

were linked to the Vp model by previously examined relationships (Gardner *et al.,* 1974; Castagna *et al.,* 1985)

Results and discussion

Velocity models obtained after WET and FWI indicate the presence of relatively higher velocity within the upper 1 km of the upper crust when compared to the starting model for ~1000 m/s (Figure 3). However, there are several regions for which the velocity remained lower (~4500 m/s). Interestingly, location of some of these upper crust, lower velocity zones correlates spatially with presence of previously mapped hydrothermal vents along the ridge axis seafloor (Von Damm 2000). This is specially valid for high-temperature (>300 ºC), focused hydrothermal discharge concentrated between 9º46’ and 9º51’N where the axial summit trough hosts two distinct vent clusters (centred at 9º46.5’ and 9º50’N), with individual vent spacing on the order of 50 to 200 m within each cluster (e.g. Fornari *et al.* 2004; Figure 1). Indeed, the slower velocities in the vicinity of the vent fields were speculated by previous ray tracing travel time tomography study (Newman *et al.,* 2010), however, due to low resolution, they have never been interpreted.

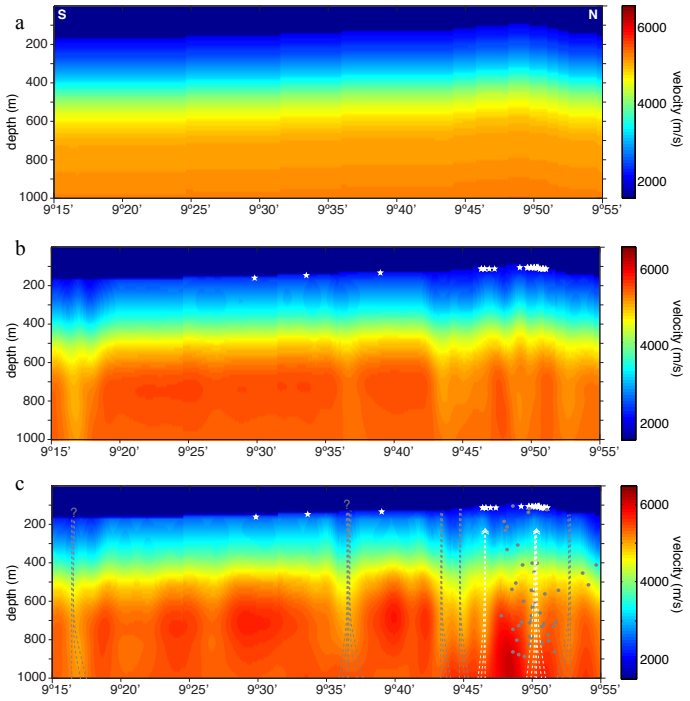

Figure 3 *Velocity models a) starting (Vera et al., 1990); b) WET after 50 iterations and c) FWI after 20 iterations. Interpretation of hydrothermal paths is superimposed with white dashed lines representing up-going path of the fluid and grey dashed lines indicating down-going flow (question mark indicates possible down-going paths); white stars indicate locations of hydrothermal vents and grey dots focus of micro earthquakes recorded during the last documented eruption (Tolstoy et al., 2006).*

Here, we suggest that the imaged lower velocity regions most probably indicate presence of up-going/down-going paths of the hydrothermal circulation as these zones besides presence of high temperature liquid, are also highly fractured. In fact, the low velocity zone centred at ~9º50’N is collocated with zone of high microseismic activity that was identified and during the last documented eruption event occurred in 2005-06 (Tolstoy *et al.,* 2006). For three individual vents located south of the eruption area, we have limited information, but it has been suggested that they are most probably inactive (Fornari *et al.,* 2012). In addition, our velocity models show no change in velocity that could indicate up-going flow beneath these individual vents. Also, it has been shown that the axial magma lens south of 9º40’N is mostly crystallised (Marjanović *et al.,* 2015), i.e. there is no heat source to sustain hydrothermal circulation in the region. However, we have to recognise that the up-going flow for the individual vents could be much narrower, below the resolution of our methods.
Also, we believe that the low velocity zone around 9º36’N (and 9º17’N) most probably represent fractured rock through which at some time in the past there was a down-going flow.
It is interesting to note that in the vicinity of the two prominent vent clusters and within the uppermost crust (up to couple of hundreds of metres) we observe slightly increased velocity (~500 m/s). One could speculate that the increase of velocity is due to mineral ore deposits as it is expected for them to extent for several hundreds of metres below vents.

Conclusions

Our results demonstrate that careful application of inversion techniques to a high-resolution seismic dataset can successfully map presence of up-going and down-going flows of hydrothermal fluids through the upper crust. However, to discriminate between preferential pathways of hydrothermal circulation, i.e. along the ridge axis or perpendicularly to it, we need to extend the inversions to 3-D.

In addition, this study shows that we could potentially image presence of important mineral accumulations within the topmost layer of the oceanic crust, but to have better insight of the potential volume, we would also need results from 3-D experiment.

Acknowledgments

We thank Suzanne M. Carbotte, John C. Mutter, Mladen Nedimović and Juan Pablo Canales, PIs and Co-PIs of the MGL0812 research cruise during which the data were collected.

References

1. Aghaei, O., Nedimović, M.R., Carton, H., Canales, J.P., Carbotte, S.M. & Mutter, J.C., 2014. Crustal thicknessand Moho character from poststack migrated 3D MCS data collected over the fast-spreading East Pacific Rise from 9º42' to 9º57'N, *Geochem. Geophys. Geosyst.,* **15**, 634–657.
2. Berryhill J.R., 1979. Wave/equation dating, *Geophysics*, vol. **44**, n. 8, 1329-1334.
Choo, J., J. Downton, and J. Dewar, 2004. Lift: A new and practical approach to noise and multiple attenuation, *First Break*, **22**, 39–44.
3. Castagna, J. P., Batzle, M. L. and Eastwood, R. L., 1985 Relationships between compressional-wave and shear-wave velocities in clastic silicate rocks. *Geophysics*, **50**, 571–581.
4. Fundis, A.T., Soule, S.A., Fornari, D.J., Perfit, M.R., 2010. Paving the seafloor: volcanic emplacement processes during the 2005–2006 eruptions at the fast spreading East Pacific Rise, 9º50'N, *Geochem. Geophys. Geosyst.*, **11**, Q08024.
5. Fornari, D.J., 2004. Submarine lava flow emplacement at the East Pacific Rise 9º50N: implications for the uppermost ocean crust stratigraphy and hydrothermal fluid circulation, in The Thermal Structure of the Ocean Crust and the Dynamics of Hydrothermal Circulation, pp. 187–217, ads German, C.R. et al., AGU.
6. Fornari, D.J., K.L. Von Damm, J.G. Bryce, J.P. Cowen, V. Ferrini, A. Fundis, M.D. Lilley, G.W. Luther III, L.S. Mullineaux, M.R. Perfit, M.F. Meana-Prado, K.H. Rubin, W.E. Seyfried Jr., T.M. Shank, S.A. Soule, M. Tolstoy, and S.M. White, 2012. The East Pacific Rise between 9°N and 10°N: Twenty-five years of integrated, multidisciplinary oceanic spreading center studies. *Oceanography* **25(1):18–43**.
7. Gardner, G., Gardner, L., and Gregory, A., 1974, Formation velocity and density-the diagnostic basics for stratigraphic traps. *Geophysics*, **39**, 770-780.
8. Levander, A., 1988. Fourth-order finite-difference P-W seismograms. *Geophysics*, **53**, 1425-1436.
9. Luo, Y., Schuster, G.T., 1991. Wave-equation travel time inversion. *Geophysics*, **56**, 645-653.
10. Marjanović, M., Carton, H., Carbotte, S.M., Nedimović, N.R., Mutter, J.C., Canales, J.P., 2015, Distribution of melt along the East Pacific Rise from 9º30' to 10ºN from an amplitude variation with angle of incidence (AVA) technique, *Geophys. J. Int.,* **203**, 1-21.
11. Newman, K., Nedimović, N.R., Delescluse, M., Menke, W., Canales, J.P., Carbotte, S.M., Carton, H., Mutter, J., 2010. East Pacific Rise axial structure from a joint tomographic inversion of traveltimes picked on downward continued and standard shot gathers collected by 3D MCS surveying, *Geophysical Research Abstracts* **Vol. 12**, EGU2010-13383.
12. Pica, A., Diet, J.P. & Tarantola, A., 1990. Nonlinear inversion of seismic reflection data in a laterally invariant medium, *Geophysics*, **55(3)**, 284–292.
13. Shipp, R. and Singh, S., 2002. Two-dimensional full wavefield inversion of wide-aperture marine seismic streamer data. *Geophys. J. Int.,* **151**, 325-344.
14. Tolstoy, M. et al., 2006. A sea-floor spreading event captured by seismometers, *Science*, **314**, 1920–1922.
15. Vera, E.E., Mutter, J.C., Buhl, P., Orcutt, J.A., Harding, A.J., Kappus, M.E., Detrick, R.S. & Brocher, T.M., 1990. The structure of 0- to 0.2-m.y.-old oceanic crust at 9ºN on the East Pacific Rise from expanded spread profiles, *J. geophys. Res.,* **95(B10)**, 15 529–15 556.
16. Von Damm, K.L., 2000. Chemistry of hydrothermal vent fluids from 9º–10º N, East Pacific Rise: "Time zero," the immediate post eruptive period, *J. Geophys. Res.,* **105**, 11 203–11 222.
17. Wang, H., Singh, S.C., and Calandra H., 2014. Integrated inversion using combined wave-equation tomography and full waveform inversion, *Geophys. J. Int.*, **138**, 1-17.